(2–10 keV) emission was seen and we place a conservative 25 mCrab upper limit on the flux of any interburst X-ray counterpart emission (1 mCrab $\approx 2 \times 10^{-11}$ erg cm^{-2} s^{-1}). One of us (C.B.M.) performs regular scanning observations of the Galactic bulge with RXTE. The closest of these were on 25 September and 2 October 2002. In both of these observations, 3σ upper limits on the X-ray flux from the source are 6 mCrab. A search of all of the Galactic bulge scans starting in February 1999 finds one scan, on 3 July 2003, in which a 15-mCrab (6.5σ) outburst was detected. However, possible confusion with other X-ray sources in the field of view ($\sim 30'$) prevents a conclusive identification. Similarly, the γ-ray source 3EG J1744–301 was detected near the position of GCRT J1745–3009 during the 1990s by the Energetic Gamma Ray Experiment Telescope, but the positional error on that source is also large ($\sim 20'$) and the source is in a highly confused region with numerous diffuse and discrete sources of γ-ray emission[25].

We next consider the possibility that the bursts from GCRT J1745–3009 could be relativistically beamed toward us, as is the case for microquasars, which are accreting black holes in binary systems that occasionally power radio-bright relativistic jets (for example GRS 1915+105, whose apparent superluminal motion has a Lorentz factor of $\gamma \approx 5$)[26,27]. It is conceivable that relativistic beaming is responsible for the high calculated brightness temperature, but the light curve of GCRT J1745–3009 does not resemble that for known microquasars or other sources of jet emission, most of which exhibit a fast rise and a slower decay and much longer timescales[3]. In addition, the apparent lack of a bright X-ray counterpart of the bursts argues strongly against accretion as the power source for the bursts.

Next, we consider radio pulsar origins for the source. A 77-min rotation period radio pulsar is excluded because the rotational energy loss rate from such a pulsar is insufficient to power the radio emission unless the magnetic field is extreme ($>10^{18}$ G) or the distance is unreasonably small (<0.5 pc). Another conceivable option is that 77 min is an orbital period and the outbursts are flux variations as a function of orbital phase similar to the pulsar PSR J0737–3039B (ref. 28). This scenario does not explain the transient behaviour from the source or the lack of interburst emission, and favours a distance of the order of 1 kpc or less.

One other class of sources to consider are magnetars, neutron stars with immense (10^{14}–10^{15} G) magnetic fields whose radiation is powered by field decay[29]. Coherent emission from the magnetosphere of a magnetar addresses the energy budget difficulties seen in the pulsar models, but all known magnetars have much shorter spin periods (~ 10 s) than the 77-min period observed for GCRT J1745–3009. An investigation of whether a new, long-period type of magnetar could produce the observed emission timescales and transient behaviour is under way (K. S. Wood, P.S.R., S.D.H., T.J.W.L. & N.E.K., manuscript in preparation). □

Received 26 November 2004; accepted 24 January 2005; doi:10.1038/nature03400.

1. Cordes, J. M., Lazio, T. J. W. & McLaughlin, M. A. The dynamic radio sky. Preprint at ⟨http://arxiv.org/abs/astro-ph/0410045⟩ (2004).
2. Hankins, T. H., Kern, J. S., Weatherall, J. C. & Eilek, J. A. Nanosecond radio bursts from strong plasma turbulence in the Crab pulsar. *Nature* **422,** 141–143 (2003).
3. Bradt, H., Levine, A., Remillard, R. & Smith, D. A. in *AIP Conf. Proc. on X-ray Astronomy: Stellar Endpoints, AGN, and the Diffuse X-ray Background* (eds White, N. E., Malaguti, G. & Palumbo, G. G. C.) **599,** 35–52 (2001).
4. Hyman, S. D., Lazio, T. J. W., Kassim, N. E. & Bartleson, A. L. Low-frequency radio transients in the galactic center. *Astron. J.* **123,** 1497–1501 (2002).
5. Hyman, S. D., Lazio, T. J. W., Kassim, N. E., Nord, M. E. & Neureuther, J. L. A search for radio transients at 0.33 GHz in the GC. *Astron. Nachr.* **324**(S1), 79–83 (2003).
6. Readhead, A. C. S. Equipartition brightness temperature and the inverse Compton catastrophe. *Astrophys. J.* **426,** 51–59 (1994).
7. Melrose, D. B. Coherent emission in AGN: a critique. *Publ. Astron. Soc. Aust.* **19,** 34–38 (2002).
8. The long wavelength array. ⟨http://lwa.nrl.navy.mil⟩ (Naval Research Laboratory, 2004).
9. Reich, W. & Fürst, E. G357.7+0.3 and G359.1−0.5—two shell-type supernova remnants in the galactic centre region. *Astron. Astrophys. Suppl. Ser.* **57,** 165–167 (1984).
10. Yusef-Zadeh, F. & Bally, J. A non-thermal axially symmetric radio wake towards the galactic centre. *Nature* **330,** 455–458 (1987).
11. Gray, A. D., Cram, L. E., Ekers, R. D. & Goss, W. M. A filamentary radio source near the galactic centre. *Nature* **353,** 237–239 (1991).
12. Nord, M. E. *et al.* High-resolution, wide-field imaging of the galactic center region at 330 MHz. *Astron. J.* **128,** 1646–1670 (2004).
13. Bastian, T. S., Bookbinder, J., Dulk, G. A. & Davis, M. Dynamic spectra of radio bursts from flare stars. *Astrophys. J.* **353,** 265–273 (1990).
14. Farrell, W. M., Desch, M. D. & Zarka, P. On the possibility of coherent cyclotron emission from extrasolar planets. *J. Geophys. Res.* **104,** 14025–14032 (1999).
15. Lazio, T. J. W. *et al.* The radiometric Bode's Law and extrasolar planets. *Astrophys. J.* **612,** 511–518 (2004).
16. Bastian, T. S., Dulk, G. A. & Leblanc, Y. A search for radio emission from extrasolar planets. *Astrophys. J.* **545,** 1058–1063 (2000).
17. Guedel, M. Stellar radio astronomy: probing stellar atmospheres from protostars to giant. *Annu. Rev. Astron. Astrophys.* **40,** 217–261 (2002).
18. Cutri, R. M. *et al. The 2MASS All-sky Catalog of Point Sources* (University of Massachusetts and Infrared Processing and Analysis Center, IPAC/California Institute of Technology, 2003).
19. Burgasser, A. J. *et al.* The spectra of T dwarfs. I. Near-infrared data and spectral classification. *Astrophys. J.* **564,** 421–451 (2002).
20. Berger, E. *et al.* Discovery of radio emission from the brown dwarf LP944-20. *Nature* **410,** 338–340 (2001).
21. Berger, E. Flaring up all over-radio activity in rapidly rotating late M and L dwarfs. *Astrophys. J.* **572,** 503–513 (2002).
22. Putman, M. E. & Burgasser, A. J. Radio emission from late-type dwarfs: quiescent emission and a spectacular radio flare from the M9 DENIS 1048-3956. *Bull. Am. Astron. Soc.* **35,** Abstr. 43.07 (2003); ⟨http://www.aas.org/publications/baas/v35n5/aas203/1159.htm⟩.
23. Dulk, G. A. & Marsh, K. A. Simplified expressions for the gyrosynchrotron radiation from mildly relativistic, nonthermal and thermal electrons. *Astrophys. J.* **259,** 350–358 (1982).
24. Bruggmann, G. & Magun, A. Temporal and spectral characteristics of the circular polarization of solar microwave bursts. *Astron. Astrophys.* **239,** 347–355 (1990).
25. Mayer-Hasselwander, H. A. *et al.* High-energy gamma-ray emission from the Galactic Center. *Astron. Astrophys.* **335,** 161–172 (1998).
26. Marscher, A. P. *et al.* Observational evidence for the accretion-disk origin for a radio jet in an active galaxy. *Nature* **417,** 625–627 (2002).
27. Fender, R. P. *et al.* Merlin observations of relativistic ejections from GRS 1915+105. *Mon. Not. R. Astron. Soc.* **304,** 365–876 (1999).
28. Lyne, A. G. *et al.* A double-pulsar system: a rare laboratory for relativistic gravity and plasma physics. *Science* **303,** 1153–1157 (2004).
29. Woods, P. M. & Thompson, C. Soft gamma repeaters and anomalous X-ray pulsars: magnetar candidates. In *Compact Stellar X-ray Sources* (eds Lewin, W. H. G. & van der Klis, M.) (in the press); preprint at ⟨http://arXiv.org/astro-ph/0406133⟩.
30. Zhao, J-H. *et al.* A transient radio source near the center of the milky way galaxy. *Science* **255,** 1538–1543 (1992).

Acknowledgements S.D.H. thanks J. Neureuther and M. Lazarova for their assistance in the Galactic Centre transient monitoring programme. We thank D. Chakrabarty, G. Denn, C. Dermer, W. Erickson, R. Remillard, K. Weiler and K. Wood for discussions. The Very Large Array (VLA) is operated by the National Radio Astronomy Observatory (NRAO), which is a facility of the National Science Foundation operated under cooperative agreement by Associated Universities. Basic research in radio astronomy is supported at Sweet Briar College by funding from the Jeffress Memorial Trust and Research Corporation. Basic research in radio and X-ray astronomy at the NRL is supported by the Office of Naval Research.

Competing interests statement The authors declare that they have no competing financial interests.

Correspondence and requests for materials should be addressed to S.D.H. (shyman@sbc.edu).

Plasma formation and temperature measurement during single-bubble cavitation

David J. Flannigan & Kenneth S. Suslick

Department of Chemistry, University of Illinois at Urbana-Champaign, Urbana, Illinois 61801, USA

Single-bubble sonoluminescence (SBSL[1–5]) results from the extreme temperatures and pressures achieved during bubble compression; calculations have predicted[6,7] the existence of a hot, optically opaque plasma core[8] with consequent bremsstrahlung radiation[9,10]. Recent controversial reports[11,12] claim the observation of neutrons from deuterium–deuterium fusion during acoustic cavitation[11,12]. However, there has been previously no strong experimental evidence for the existence of a

plasma during single- or multi-bubble sonoluminescence. SBSL typically produces featureless emission spectra[13] that reveal little about the intra-cavity physical conditions or chemical processes. Here we report observations of atomic (Ar) emission and extensive molecular (SO) and ionic (O_2^+) progressions in SBSL spectra from concentrated aqueous H_2SO_4 solutions. Both the Ar and SO emission permit spectroscopic temperature determinations, as accomplished for multi-bubble sonoluminescence with other emitters[14–16]. The emissive excited states observed from both Ar and O_2^+ are inconsistent with any thermal process. The Ar excited states involved are extremely high in energy (>13 eV) and cannot be thermally populated at the measured Ar emission temperatures (4,000–15,000 K); the ionization energy of O_2 is more than twice its bond dissociation energy, so O_2^+ likewise cannot be thermally produced. We therefore conclude that these emitting species must originate from collisions with high-energy electrons, ions or particles from a hot plasma core.

In order to gain insight into the physical conditions and chemical processes occurring during single-bubble cavitation, we have explored a variety of low-volatility liquids[17], observing both stationary and moving SBSL. We have now discovered the generation of extremely intense SBSL from a moving single bubble in concentrated aqueous H_2SO_4 solutions, H_2SO_4(aq.), which have very low vapour pressures[18] and are essentially transparent down to a wavelength of 200 nm. Under optimal conditions, the SBSL intensity from 85 wt% H_2SO_4(aq.) under Ar is increased 2,700 times compared to that from water under Ar, and the intensity under Xe is increased 1,500 times compared to water under Xe (Fig. 1). When Xe is dissolved in degassed 85% H_2SO_4(aq.), the SBSL is, by more than two orders of magnitude, the most intense yet observed in any liquid. SBSL from H_2SO_4 solutions had been previously reported, but with only a few-fold increase in intensity compared to water[19].

Bright SBSL spectra from concentrated H_2SO_4(aq.) are similar to water SBSL spectra, consisting of a featureless continuum that increases towards the ultraviolet (UV). Although these spectra are much more intense, blackbody fits (which have been previously reported for SBSL in water[20]) do not yield vastly different temperatures for the SBSL now observed from H_2SO_4(aq.); all four spectra in Fig. 1 have an apparent blackbody temperature of ~12,500 ± 1,500 K. The very marked increase in SBSL intensity seen from concentrated H_2SO_4(aq.) is due in part to the much lower concentration of polyatomic species inside the bubble relative to water at the same temperature: less of the energy of cavitation is consumed by endothermic bond dissociations[21]. The remaining bubble contents, comprised almost entirely of noble gas atoms mixed with a small amount of H_2SO_4 vapour, must therefore absorb a larger portion of the energy of collapse.

Importantly, the parameter space that supports SBSL in H_2SO_4(aq.) is much larger than in water, with SBSL observable over an acoustic pressure range of 1.3 to >6 bar. (The acoustic pressures are estimated from hydrophone measurements at the centre of the acoustic field; movement of the bubble about the

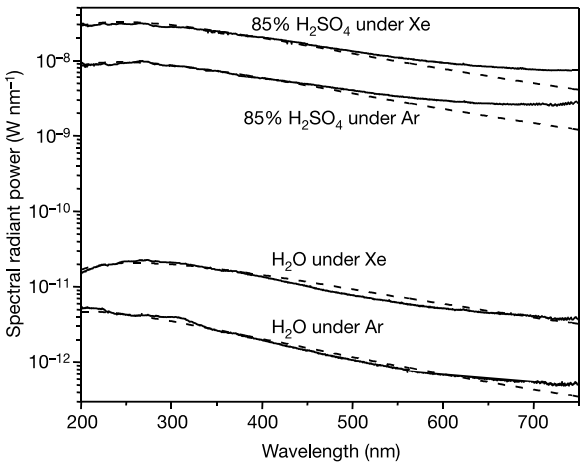

Figure 1 SBSL spectra from 85% H_2SO_4(aq.) and pure water regassed with Xe and Ar (solid lines); apparent fits to blackbody spectra are given as dashed lines. Noble gas content of solutions, acoustic frequency and acoustic pressure were adjusted to obtain the brightest SBSL emission. The SBSL apparatus, spectral acquisition system and acoustic pressure measurements have been previously described[17]. All spectra were corrected for solution and resonator absorption, and for the response of the optical system (against NIST traceable standard lamps).

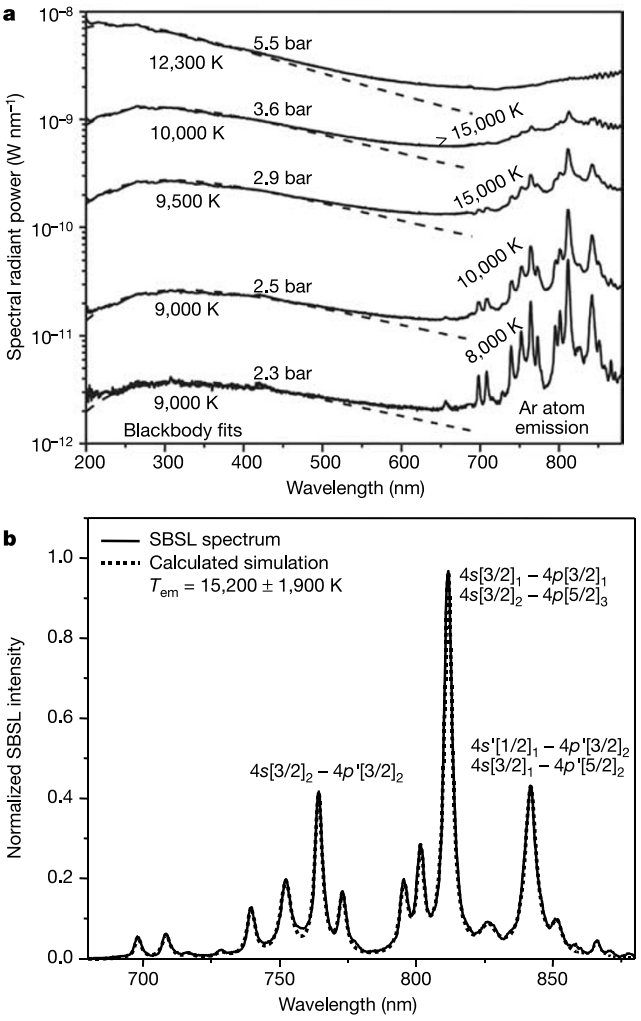

Figure 2 SBSL spectra from 85% H_2SO_4(aq.). **a**, Solid lines are the observed SBSL emission spectra, dashed lines are calculated blackbody spectra. Applied acoustic pressures are shown above their corresponding plot. Temperatures of blackbody fits and of Ar atom emission (compare with **b**) are shown next to their corresponding plot. The strong neutral Ar atom emission lines in the red and near-infrared region of the spectra arise from the 4*s*–4*p* manifold. The 4*s* state is situated 11.5–11.8 eV above the ground state (3*p*), whereas the 4*p* state lies 13.1–13.5 eV above the ground state. **b**, Ar atom line emission (2.8 bar; solid line) compared to a calculated Ar atom emission spectrum at 15,200 K (dashed line). The underlying continuum has been subtracted; spectra are normalized to intensity at 811 nm. The most prominent lines are labelled with the corresponding transitions. The lines at 811 and 840 nm each contain contributions from two relatively strong transitions.

pressure antinode will decrease the effective acoustic pressure experienced by the bubble, so acoustic pressures given here are upper limits.) In SBSL from more weakly driven bubbles, for example, we observe very strong atomic emission from neutral Ar (Fig. 2). In this case, as the driving acoustic pressure is increased, the intensity of Ar emission lines decreases relative to the continuum emission, and the Ar lines broaden gradually into unresolved peaks at >5 bar. Observation of emission from excited states of atomic Ar allows us to calculate emission temperatures from the well-known energy levels, transition probabilities, statistical weights, and photon energies of Ar (ref. 22). Ar atom emission temperatures generated during SBSL from 85% H_2SO_4(aq.) were observed to increase with increasing acoustic pressure, and were found to be 8,000 ± 1,000 K at 2.3 bar, 10,700 ± 1,300 K at 2.5 bar, and 15,200 ± 1,900 K at 2.8 bar. Note that these experimentally determined temperatures are consistent with theoretically predicted SBSL temperatures[7,23]. At higher acoustic pressures, accurate fits to Ar emission spectra become difficult owing to line broadening and the development of line asymmetries, possibly due to increased Ar ion concentrations. At the highest acoustic pressures reached before the bubble was forced from the centre of the resonator (>6 bar), calculation of SBSL temperature was impossible owing to the extreme broadening of all spectral features.

We note especially that the Ar excited states that are being populated are extremely high in energy (>13 eV)[24], which is too high to be populated thermally at the <1 eV effective emission temperature of Ar. This provides, to our knowledge, the first experimental evidence for excitation via high-energy particle collisions (for example, electron impact on Ar) from a hot plasma core. The possibility of an optically opaque, highly ionized plasma core during SBSL has been previously suggested by calculations[8]. Similar circumstances occur during intense shockwave heating in gases. For example, the limiting emission temperature of an intense shockwave in air is only ~17,000 K (ref. 25), which represents the opacity limit of shock heating of air, and shock-heated Ar plasmas typically have line emission temperatures below ~20,000 K (ref. 26).

Comparisons of Ar atom emission temperatures to blackbody fits of the UV continuum (Figs 1 and 2a) are problematic for several reasons. First, the origin of the UV continuum emission is unclear: it may be partially blackbody radiation from the emitting shell surrounding an optically opaque core[6,7], and partially bremsstrahlung due to ionization[9,10,27]. It could also be due to ion–electron recombination, which is likely to be present in a dense plasma[9,10]. Furthermore, the continuum emission and the well-resolved Ar atom emission do not necessarily originate at the same time during bubble collapse or from the same spatial region within the bubble. A simple blackbody fit under these circumstances is unlikely to produce an accurate temperature measurement, and further comparison is therefore unwarranted.

According to current theoretical models of SBSL, compressional heating of the bubble should show some dependence on the thermal conductivity of the gas within the bubble[23,28]. As shown in Fig. 3, we can use mixtures of Ar and Ne to systematically control the emission temperature from >15,000 K down to ~1,500 K. The effects of thermal conductivity may come both from direct thermal transport and from changes in the size of the plasma core[8,23,25]. Thus it is clear that bubble collapse is only approximately adiabatic, and that even in SBSL, thermal conductivity of the dissolved gases is a critical experimental parameter.

We also observe extensive vibronic progressions arising from the $B^3\Sigma^- – X^3\Sigma^-$ system of sulphur monoxide (SO; ref. 29) in the SBSL spectra of concentrated H_2SO_4(aq.). Sulphur monoxide vibronic progressions are most prominent when the H_2SO_4(aq.) solution contains dissolved Ne (Fig. 4a). The bands are very weakly present in SBSL spectra of a very dimly luminescing Ar bubble, and they are totally absent from SBSL spectra of Kr and Xe bubbles, no matter how dim. If heat is rapidly conducted out of a Ne-filled bubble during collapse, dissociation of SO will occur to a lesser degree, resulting in an increase in SO emission intensity, as observed.

By comparing relative intensities of inter-progression SO emission bands, and also by observing how relative intensities of the bands change with increasing acoustic pressure, effective SO temperatures were determined to be 1,580 ± 110 K at 3.3 bar, 2,470 ± 170 K at 4.2 bar, and 3,480 ± 240 K at 5.1 bar, all regassed with Ne. At higher acoustic pressures, the emission temperatures continue to increase and become difficult to determine, owing to the blending of bands and the decrease in SO emission intensity (as dissociation occurs). Note that at the highest acoustic pressures applied (>6 bar), features of SO molecular emission were still apparent in the spectra. Emission temperatures from SO are of course limited by its dissociation, and so may represent either

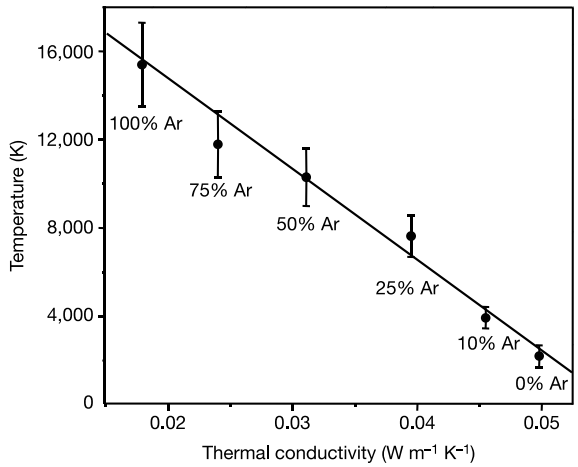

Figure 3 Emission temperatures of SBSL of 85% H_2SO_4(aq.) regassed with Ar/Ne mixtures (acoustic pressure 3 bar) are shown as a function of the thermal conductivity of the gas mixtures. Temperatures were calculated from Ar atom emission for all but the 100% Ne measurement, whose temperature was determined from SO emission (compare Fig. 4). Error bars are determined from the errors in the transition probabilities reported in ref. 20, and from an estimated 5% experimental error in the measured temperature.

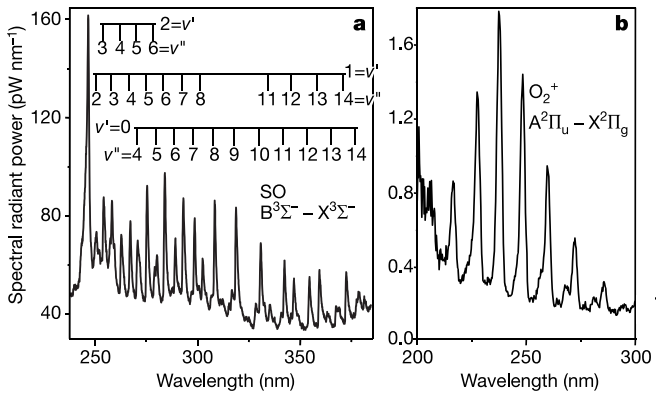

Figure 4 Vibronic progressions in SBSL spectra. **a**, Sulphur monoxide (SO) ($B^3\Sigma^- – X^3\Sigma^-$) emission from 85% H_2SO_4(aq.) regassed with Ne. The intense peak near 250 nm arises from the SO ultraviolet system ($A^3\Pi – X^3\Sigma^-$; ref. 29). Vibrational levels in the $B^3\Sigma^-$ state are denoted by v' while vibrational levels in the $X^3\Sigma^-$ state are denoted by v''. **b**, Dioxygenyl cation (O_2^+) ($A^2\Pi_u – X^2\Pi_g$) emission[30] from 85% H_2SO_4(aq.) regassed with O_2/Xe.

emission from outer regions of the collapsing bubble or early (or late) times during bubble collapse.

Confirmation of the presence of a plasma in the collapsing bubble comes from the observation of O_2^+ emission[30] (Fig. 4b). The bond energies of O_2 and O_2^+ are 5.1 and 6.5 eV, respectively, while the ionization energy of O_2 is much higher at 12.1 eV. A total of over 18 eV of energy is necessary to form excited O_2^+. The formation and excitation of O_2^+ therefore cannot occur thermally, and probably occurs via high-energy electron impact from the hot, opaque plasma core. To our knowledge, this is the first example of emission from any ion in any sonoluminescence spectrum under any conditions. □

Received 15 September 2004; accepted 17 January 2005; doi:10.1038/nature03361.

1. Barber, B. P. & Putterman, S. J. Light scattering measurements of the repetitive supersonic implosion of a sonoluminescing bubble. *Phys. Rev. Lett.* **69,** 3839–3842 (1992).
2. Gompf, B., Günther, R., Nick, G., Pecha, R. & Eisenmenger, W. Resolving sonoluminescence pulse width with time-correlated single photon counting. *Phys. Rev. Lett.* **79,** 1405–1408 (1997).
3. Gaitan, D. F., Crum, L. A., Church, C. C. & Roy, R. A. Sonoluminescence and bubble dynamics for a single, stable, cavitation bubble. *J. Acoust. Soc. Am.* **91,** 3166–3183 (1992).
4. Lohse, D., Brenner, M. P., Dupont, T. F., Hilgenfeldt, S. & Johnston, B. Sonoluminescing air bubbles rectify argon. *Phys. Rev. Lett.* **78,** 1359–1362 (1997).
5. Brenner, M. P., Hilgenfeldt, S. & Lohse, D. Single-bubble sonoluminescence. *Rev. Mod. Phys.* **74,** 425–484 (2002).
6. Moss, W. C., Clarke, D. B. & Young, D. A. Calculated pulse widths and spectra of a single sonoluminescing bubble. *Science* **276,** 1398–1401 (1997).
7. Moss, W. C. *et al.* Computed optical emissions from a sonoluminescing bubble. *Phys. Rev. E* **59,** 2986–2992 (1999).
8. Burnett, P. D. S. *et al.* Modeling a sonoluminescing bubble as a plasma. *J. Quant. Spectrosc. Radiat. Transfer* **71,** 215–223 (2001).
9. Hilgenfeldt, S., Grossmann, S. & Lohse, D. A simple explanation of light emission in sonoluminescence. *Nature* **398,** 402–405 (1999).
10. Yasui, K. Mechanism of single-bubble sonoluminescence. *Phys. Rev. E* **60,** 1754–1758 (1999).
11. Taleyarkhan, R. P. *et al.* Evidence for nuclear emissions during acoustic cavitation. *Science* **295,** 1868–1873 (2002).
12. Taleyarkhan, R. P. *et al.* Additional evidence of nuclear emissions during cavitation. *Phys. Rev. E* **69,** 036109 (2004).
13. Hiller, R., Weninger, K., Putterman, S. J. & Barber, B. P. Effect of noble gas doping in single-bubble sonoluminescence. *Science* **266,** 248–250 (1994).
14. McNamara, W. B. III, Didenko, Y. T. & Suslick, K. S. Sonoluminescence temperatures during multi-bubble cavitation. *Nature* **401,** 772–775 (1999).
15. Flint, E. B. & Suslick, K. S. The temperature of cavitation. *Science* **253,** 1397–1399 (1991).
16. Didenko, Y. T., McNamara, W. B. III & Suslick, K. S. Effect of noble gases on sonoluminescence temperatures during multibubble cavitation. *Phys. Rev. Lett.* **84,** 777–780 (2000).
17. Didenko, Y. T., McNamara, W. B. III & Suslick, K. S. Molecular emission from single-bubble sonoluminescence. *Nature* **407,** 877–879 (2000).
18. Greenewalt, C. H. Partial pressures of aqueous solutions of sulfuric acid. *J. Ind. Eng. Chem.* **17,** 522–523 (1925).
19. Troia, A., Ripa, D. M. & Spagnolo, R. in *World Congress on Ultrasonics* (ed. Cassereau, D.) 1041–1044 (Société Française d'Acoustique, Paris, 2003).
20. Vazquez, G., Camara, C., Putterman, S. & Weninger, K. Sonoluminescence: Nature's smallest blackbody. *Opt. Lett.* **26,** 575–577 (2001).
21. Didenko, Y. T. & Suslick, K. S. The energy efficiency of formation of photons, radicals and ions during single-bubble cavitation. *Nature* **418,** 394–397 (2002).
22. Wiese, W. L., Brault, J. W., Danzmann, K., Helbig, V. & Kock, M. Unified set of atomic transition probabilities for neutral argon. *Phys. Rev. A.* **39,** 2461–2471 (1989).
23. Toegel, R. & Lohse, D. Phase diagrams for sonoluminescing bubbles: A comparison between experiment and theory. *J. Chem. Phys.* **118,** 1863–1875 (2003).
24. Cooper, R., Grieser, F., Sauer, M. C. Jr & Sangster, D. F. Formation and decay kinetics of the 2p levels of neon, argon, krypton, and xenon produced by electron-beam pulses. *J. Phys. Chem.* **81,** 2215–2220 (1977).
25. Zel'dovich, Y. B. & Raizer, Y. P. *Physics of Shock Waves and High-Temperature Hydrodynamic Phenomena* (Academic, New York, 1966).
26. Tourin, R. H. *Spectroscopic Gas Temperature Measurement* (Elsevier, Amsterdam, 1966).
27. Camara, C., Putterman, S. & Kirilov, E. Sonoluminescence from a single bubble driven at 1 megahertz. *Phys. Rev. Lett.* **92,** 124301 (2004).
28. Yasui, K. Single-bubble sonoluminescence from noble gases. *Phys. Rev. E* **63,** 035301 (2001).
29. Ajello, J. M. *et al.* Middle ultraviolet and visible spectrum of SO_2 by electron impact. *J. Geophys. Res. Space* **107,** SIA2 (2002).
30. Schappe, R. S., Schulman, M. B., Sharpton, F. A. & Lin, C. C. Emission of the O_2^+ ($A^2\Pi_u \rightarrow X^2\Pi_g$) second-negative-band system produced by electron impact on O_2. *Phys. Rev. A* **38,** 4537–4545 (1988).

Acknowledgements This work was supported by the National Science Foundation and the US Defense Advanced Research Projects Agency. We acknowledge conversations with F. Grieser on the mechanism of Ar atom emission, and with L. A. Crum, D. Lohse, W. C. Moss and S. J. Putterman.

Competing interests statement The authors declare that they have no competing financial interests.

Correspondence and requests for materials should be addressed to K.S.S. (ksuslick@uiuc.edu).

Self-directed self-assembly of nanoparticle/copolymer mixtures

Yao Lin[1]*, Alexander Böker[1]*†, Jinbo He[1], Kevin Sill[1], Hongqi Xiang[1], Clarissa Abetz[2], Xuefa Li[3], Jin Wang[3], Todd Emrick[1], Su Long[4], Qian Wang[4], Anna Balazs[5] & Thomas P. Russell[1]

[1]*Department of Polymer Science & Engineering, University of Massachusetts, Amherst, Massachusetts 01003, USA*
[2]*Bayreuther Institut für Makromolekülforschung, Universität Bayreuth, 95440 Bayreuth, Germany*
[3]*Advanced Photon Source, Argonne National Laboratory, Argonne, Illinois 60439, USA*
[4]*Department of Chemistry, University of South Carolina, Columbia, South Carolina 29208, USA*
[5]*Department of Chemical and Petroleum Engineering, University of Pittsburgh, Pittsburgh, Pennsylvania 15261, USA*

* These authors contributed equally to this work
† Present address: Lehrstuhl für Physikalische Chemie II, Universität Bayreuth, 95440 Bayreuth, Germany

The organization of inorganic nanostructures within self-assembled organic or biological templates[1–11] is receiving the attention of scientists interested in developing functional hybrid materials. Previous efforts have concentrated on using such scaffolds[7,9,12] to spatially arrange nanoscopic elements as a strategy for tailoring the electrical, magnetic or photonic properties[8–11,13–16] of the material. Recent theoretical arguments[16–18] have suggested that synergistic interactions between self-organizing particles and a self-assembling matrix material can lead to hierarchically ordered structures. Here we show that mixtures of diblock copolymers and either cadmium selenide- or ferritin-based nanoparticles exhibit cooperative, coupled self-assembly on the nanoscale. In thin films, the copolymers assemble into cylindrical domains, which dictate the spatial distribution of the nanoparticles; segregation of the particles to the interfaces mediates interfacial interactions and orients the copolymer domains normal to the surface, even when one of the blocks is strongly attracted to the substrate. Organization of both the polymeric and particulate entities is thus achieved without the use of external fields[10,19], opening a simple and general route for fabrication of nanostructured materials with hierarchical order.

Block copolymer/nanoparticle films were prepared by spin-coating toluene solutions of a mixture of 3- or 5-wt% polystyrene-*block*-poly(2-vinylpyridine) copolymer, denoted PS-*b*-P2VP, and 1-wt% tri-*n*-octylphosphine oxide-(TOPO)-covered CdSe nanoparticles (4 nm in diameter) onto silicon wafers. The 150–600-nm-thick films were annealed thermally at 170 °C under vacuum, in a supercritical fluid CO_2 environment at 70 °C, or in chloroform vapours at room temperature (see Supplementary Information). Each treatment imparts mobility to the thin film mixtures, allowing them to attain an equilibrium morphology within about two days. We note that the TOPO-covered CdSe nanoparticles are stable at the temperatures used, such that aggregation caused by ligand disassociation was not observed. Films of the pure diblock copolymer and the block copolymer mixed with TOPO were prepared and used as controls to assess the influence of the nanoparticles on the thin-film behaviour.

Figure 1a and b show scanning force microscopy (SFM) height and phase images of a 400-nm-thick PS-*b*-P2VP film spin-coated from toluene and dried. An array of microphase-separated domains of P2VP in a PS matrix, similar to those found in previous investigations[20,21], is seen. The phase image maps onto the height variations from the topography of the sample. Upon thermal annealing at 170 °C for two days, the equilibrium morphology of